Inorganic Chemistry

Article

pubs.acs.org/IC

Turn Helical Motifs from Pair to Single Entangled Double Helixes in a Cobalt–Vanadate System via Introduction of a V-Shaped Ligand

Shaobin Li, Wenlong Sun, Kun Wang, Huiyuan Ma,* Haijun Pang,* Heng Liu, and Jianxin Zhang

Key Laboratory of Green Chemical Engineering and Technology of College of Heilongjiang Province, College of Chemical and Environmental Engineering, Harbin University of Science and Technology, Harbin 150040, China

Supporting Information

ABSTRACT: Two novel helical compounds based on polyoxovanadates, $[Co(H_2O)_2V_2O_6]$ (**1**) and [Co(bimb)-V_2O_6] (**2**) (bimb =1,3-bis(1-imidazoly)benzene), have been synthesized under identical hydrothermal conditions, providing two structurally different helical motifs due to introduction of a V-shaped bimb ligand in **2**. Compound **1** possesses a pair of entanglement double helixes in a 3D inorganic framework, whereas compound **2** shows a single entangled double helix in a 3D inorganic–organic network owing to the influences of steric hindrance of ligands as well as coordination geometries of metal cations. The electrocatalytic and photocatalytic properties of **1** and **2** were also investigated in details.

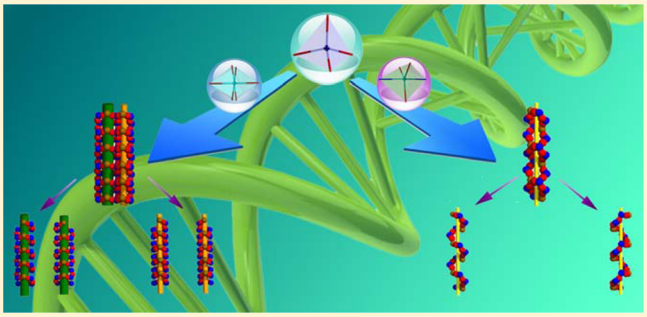

INTRODUCTION

Helical structures as the foundation of the genetic code are ubiquitous in nature. In recent years, the helical structures have been attracting increased attention in materials chemistry and coordination chemistry. Until now, thanks to the work of chemists, many novel artificial helical compounds have been rationally designed and synthesized,[1] which show significance in multidisciplinary areas such as asymmetric catalysis, biology, and optical devices.[2] Polyoxometalates (POMs), as a unique class of metal-oxide clusters with a vast structural diversity, possess a wide range of potential applications from catalysis and material science to medicine.[3−14] From a structural point of view, the incorporation of POMs into helical system leading to the formation of the helical compounds based on POMs is very interesting, since there exists a correlation between structural complexity and multifunctionality in coordination compounds.[15] These facts have provided a powerful impetus for the creation of helical compounds based on POMs. An excellent example of the helical compounds based on POMs is the first inorganic double helixes self-assembled from simple starting materials under hydrothermally conditions reported by Haushalter and Zubieta et al.[16] Subsequently, various helical compounds based on POMs with intriguing structural topologies have been obtained in recent years. However, in contrast to other rapidly increased coordination compounds, the helical compounds based on POMs have been seldom observed, and for the sake of comparison, these compounds can be roughly divided to three types according to number of helixes and their entangled styles: (I) right- or/and left-handed single helix,[17] (II) entangled right- and left-handed double helixes without entanglement nodes,[18] and (III) a single of entangled right- and left-handed double helixes with entanglement nodes.[19] Among the three types of helical compounds based on POMs, the first one is very common, whereas the last two types are rarely observed. Within our knowledge, only 16 compounds belonging to types II or III have been reported until now (see Table S1, Supporting Information). The construction of helical compounds based on POMs toward a specific disposition in II, III, or new types has therefore remained an intriguing challenge for chemists.

As a ramification of POMs, due to the variable oxidation states of vanadium (III, IV, and V) as well as multiform coordination geometries of vanadium oxide polyhedra (tetrahedrons, square pyramids, trigonal bipyramids, and octahedra), polyoxovanadates (POVs) with tunable redox, catalytic, and photochemical properties can be self-condensed by vanadium oxide polyhedra to form a variety of clusters including di-,[20] tri-,[21] tetra-,[22] penta-,[23] deca-,[24] dodeca-,[25] trideca-,[26] pentadeca-,[27] hexadeca-,[28] heptadeca-,[29] octadeca-,[30] and so on. Hence, the POVs can be viewed as transferable synthons for the synthesis of novel helixes. In addition, Hong et al. recently pointed out that the use of V-shaped ligands as structure-directing agents is an effective approach to obtain helical structures with ease.[31] Taking this into account, first, by choosing NH_4VO_3 as vanadium source to form POVs in situ, $Co(CH_3COO)_2{\cdot}4H_2O$ as metal ions source, and triethylamine as the mineralization agent, we hydrothermally synthesized a helical compound based on POVs, $[Co(H_2O)_2V_2O_6]$ (**1**). Compound **1** shows an unprecedented helical disposition type (IV), namely, a pair of right- and left-handed double helixes with entanglement nodes (Scheme 1). Furthermore, by

Received: January 28, 2014
Published: April 16, 2014

   dx.doi.org/10.1021/ic500224m | *Inorg. Chem.* 2014, 53, 4541−4547

Scheme 1. Schematic Representation of the Four Types of Helical Structures (I–IV)

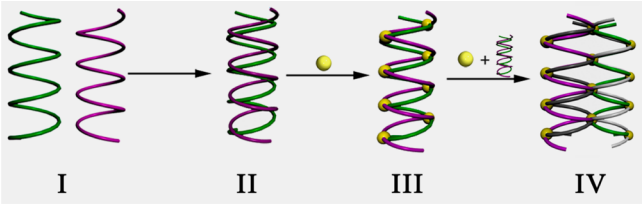

introducing the V-shape bimb ligand (bimb =1,3-bis(1-imidazoly)benzene) into the reaction system without other conditions changed, compound **2** ($[Co(bimb)V_2O_6]$) with structurally different helical motifs was obtained. Compound **2** exhibits a single of entangled double helixes, but its helixes are deposited in type III (Scheme 1). The distinct structural features of these two compounds suggest that the steric hindrance of ligands as well as coordination geometries of metal cations should have great effect on the structures of the title compounds, and these influences are discussed in this paper. The electrocatalytic and photocatalytic properties of **1** and **2** were also investigated.

EXPERIMENTAL SECTION

Materials and General Methods. All reagents and solvents for syntheses were purchased from commercial sources and used as received without further purification. The elemental analyses were of C, H, and N conducted on a Perkin Elmer 240C elemental analyzer and those of V and Co were analyzed on a PLASMA-SPEC(I) ICP atomic emission spectrometer. The IR spectra were recorded in the range of 4000–400 cm^{-1} on an Alpha Centaurt FT/IR spectrophotometer using KBr pellets. The X-ray powder diffraction (XRPD) patterns were recorded with a Siemens D5005 diffractometer with Cu Kα (λ = 1.5418 Å) radiation. A CHI 760D electrochemical workstation was used for control of the electrochemical measurements and data collection. A conventional three-electrode system was used, with a modified carbon paste electrode (CPE) as a working electrode, a twisted platinum wire as counter electrode, and a commercial Ag/AgCl as a reference electrode. UV–vis absorption spectra were recorded on a 756 CRT UV–vis spectrophotometer.

Syntheses of Compounds 1 and 2. *$[Co(H_2O)_2V_2O_6]$ (1).* A mixture of NH_4VO_3 (187 mg, 1.6 mmol), $Co(CH_3COO)_2{\cdot}4H_2O$ (149 mg, 0.8 mmol), and triethylamine (0.1 mL) was dissolved in 10 mL of distilled water at room temperature. The pH value was adjusted to about 5 by 1.0 M HCl solution, and then the solution was transferred and sealed in a 25 mL Teflon-lined stainless steel container and kept at 160 °C for 4 days. After slow cooling to room temperature at a rate of 10 °C·h^{-1}, red crystals of **1** were obtained (Figure S1, Supporting Information) (42% yield based on Co). The final pH value of the solution after the reaction is approximate to 4.5. Elemental analyses Calcd for $CoH_4O_8V_2$ (292.84): Co, 20.13; H, 1.38; V, 34.80. Found: Co, 20.44; H, 1.41; V, 34.58.

$[Co(bimb)V_2O_6]$ (2). The synthetic method was similar to that of **1**, except that the bimb (72 mg, 0.8 mmol) is introduced into the reaction system of **1**. Dark red crystals of **2** were obtained (Figure S2, Sipporting Information) (35% yield based on Co). The final pH value of the solution after the reaction is approximately 4.1. Anal. Calcd for $C_{12}H_{10}CoN_4O_6V_2$ (467.05): C, 30.84; H, 2.16; N, 12.00; V, 21.82; Co, 12.62. Found: C, 30.63; H, 2.07; N, 12.14; V, 21.43; Co, 12.84.

X-ray Crystallography. Single-crystal X-ray diffraction datas for **1** and **2** were recorded on a Bruker Apex CCD diffractometer with graphite-monochromated Mo Kα radiation (λ = 0.71069 Å). Absorption corrections were applied using multiscan techniques. All the structures were solved by direct methods using SHELXS-97[32a] and refined by full-matrix least-squares techniques using the SHELXL-97 program[32b] within WINGX.[32c] The hydrogen atoms of water molecule for the compound **1** could be positioned reliably. The hydrogen atoms of the organic ligands for the compound **2** were refined as rigid groups. The detailed crystallographic data and structure refinement parameters are summarized in Table 1. CSD-427193 (**1**) and CCDC-979058 (**2**) contain supplementary crystallographic data for this paper.

Table 1. Crystal Data and Structure Refinements for 1 and 2[a]

	1	2
formula	$CoH_4O_8V_2$	$C_{12}H_{10}CoN_4O_6V_2$
M	292.84	467.05
crystal system	orthorhombic	triclinic
space group	*Pnma*	*P*-1
a (Å)	5.5676(14)	7.981(5)
b (Å)	10.692(3)	8.672(5)
c (Å)	11.859(3)	11.828(5)
V (Å^3)	706.0(3)	757.8(7)
α (deg)	90	104.092(5)
β (deg)	90	97.985(5)
γ (deg)	90	102.840(5)
Z	4	2
D_{calcd} (g cm^{-3})	2.755	2.047
T (K)	273(2)	293(2)
μ (mm^{-1})	4.914	2.330
reflns measured	5152	6116
reflns unique	924	3805
R_{int}	0.0417	0.0175
GoF on F^2	0.959	1.039
R_1/wR_2 [$I \geq 2\sigma(I)$]	0.0250/0.0673	0.0333/0.0791

[a] $R_1 = \sum||F_0| - |F_c||/\sum|F_0|$, $wR_2 = \sum[w(F_0^2 - F_c^2)^2]/\sum[w(F_0^2)^2]^{1/2}$.

RESULTS AND DISCUSSION

Bond valence sum calculations[33] show that all vanadium atoms are in +V oxidation states, and cobalt atoms are in +II oxidation states in **1** and **2**. This result is consistent with structural analyses and charge balance.

Structure Description of Compound 1. Single-crystal X-ray diffraction analysis reveals that **1** crystallizes in the orthorhombic space group *Pnma* (No. 62) and consists of a Co^{2+} cation, $[V_2O_6]^{2-}$ cluster, and two coordinated water molecules (Figure 1). The Co^{2+} cation and two water molecules (O_{W1} and O_{W2}) lie at the sites with crystallographically imposed mirror symmetry. The Co(1) atom is six-

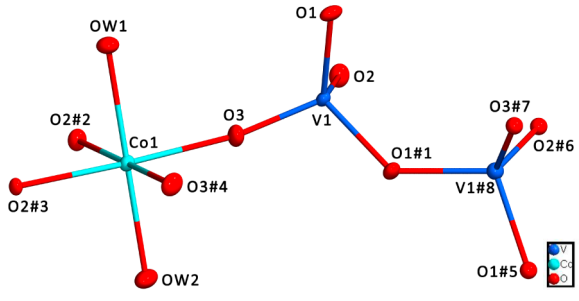

Figure 1. ORTEP diagram (at 30% probability level) of the basic building blocks in **1** and the coordination environment for the $[V_2O_6]^{2-}$ cluster and Co^{2+} ion in **1** (the H atoms of coordinated water molecules are omitted for clarity, symmetry codes: (1) 0.5 + x, y, 1.5 − z; (2) −x, 1 − y, 2 − z; (3) −x, 0.5 + y, 2 − z; (4) x, 1.5 − y, z; (5) 1 + x, y, z; (6) 0.5 + x, y, 1.5 − z; (7) 0.5 + x, y, 1.5 − z; (8) 0.5 + x, y, 1.5 − z).

dx.doi.org/10.1021/ic500224m | Inorg. Chem. 2014, 53, 4541–4547

coordination in an elongated octahedral geometry (Figure 1), defined by six oxygen atoms from two water molecules and four $\{VO_4\}$ tetrahedra, displaying Jahn−Teller (JT) elongation axes with the two JT bonds being at least 0.5 Å longer than the other four bonds. The average of Co−O bond lengths is ca. 2.075 Å, and the O−Co−O angles range from 85.72(11)° to 179.88(11)°. In the $[V_2O_6]^{2-}$ cluster, there is one crystallographically independent V atom. The V(1) atom, residing in a distorted tetrahedral environment, is coordinated by four bridging oxygen atoms from one $\{Co(H_2O)_2O_4\}$ octahedron and three identical $\{VO_4\}$ tetrahedral (Figure 1). The V−O bond lengths range from 1.634(17) to 1.803(17) Å, and the average distance of V−O bond lengths is ca. 1.722 Å.

Compound **1** is the first example of the helical compound based on POMs that possesses a pair of double helixes with entanglement nodes in a 3D inorganic framework, which belongs to an unprecedented helical disposition type (IV) (Scheme 1). Such an intricate structure can be described in the following two steps: first, the $\{Co(H_2O)_2O_4\}$ octahedra and $\{VO_4\}$ tetrahedra are connected alternately to each other by sharing oxygen atoms to form a pair of different entangled double helixes (**I** and **II**) running along the *a* axis (see details in Figures 2 and 3). Each of the double helixes consists of two

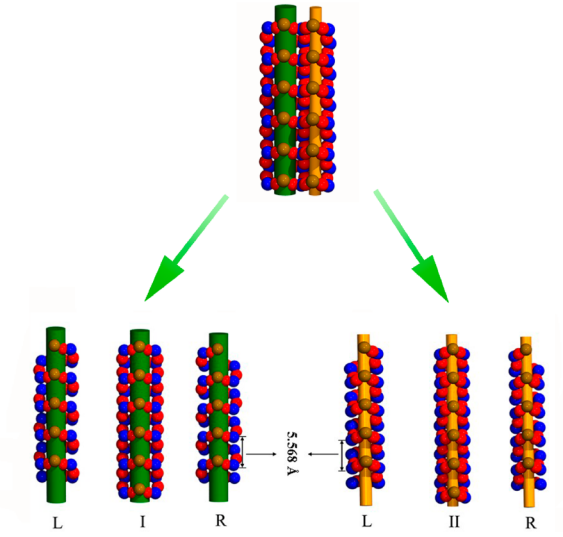

Figure 2. Detailed view of the two pair of entangled double helical chains in **1**. Color code: Co, dark yellow; V, blue; O, red. For clarity, only the Co−O−V−O−V−O−Co backbone is shown.

interweaved right- and left-handed helixes by sharing cobalt, vanadium, and oxygen atoms; thus, there are four kinds of helixes with an identical screw-pitch of ca. 5.568 Å. Interestingly, as shown in Figure 3b, the entangled double helixes (**I** and **II**) are arranged regularly along their screw axes to construct two kinds of approximately elliptical cylinders (**A** and **B**) with 1D helical channels. The cross-section dimensions of cylinders are ca. 5.7 × 6.9 Å^2 for **A** and ca. 4.6 × 7.4 Å^2 for **B**, respectively. In the second step, the different double helixes are further connected by corner-sharing vanadium and oxygen atoms to achieve a 2D layer (Figure 3c), and the adjacent layers are further connected each other by corner-sharing cobalt atoms to form a 3D inorganic framework (Figure 3d and Figure S3, Supporting Information). The topological analysis of the structure has been performed by considering each $\{VO_4\}$ tetrahedron as a 4-connected node and each $\{Co(H_2O)_2O_4\}$

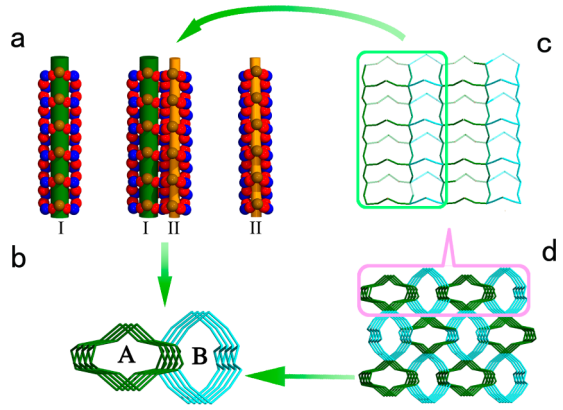

Figure 3. View of the two pairs of entangled double helical chains (**I** and **II**) (a), two kinds of approximately elliptical cylinders (**A** and **B**) with 1D helical channels (b), a 2D layer connected by the double helixes via corner-sharing vanadium and oxygen atoms (c), and a 3D inorganic framework (d). For clarity, only the Co−O−V−O−V−O−Co backbone is shown.

octahedron as a 4-connected node, respectively. Hence, the 3D framework of **1** can be simplified as a (4,4)-connected net with a $(8^1\ 12^4\ 16^1)(8^2\ 12^2\ 16^2)$ topology (the first symbol for a $\{VO_4\}$ tetrahedron and the second for a $\{Co(H_2O)_2O_4\}$ octahedron, Figure S4, Supporting Information).

Structure Description of Compound 2. Single-crystal X-ray diffraction analysis reveals that **2** crystallizes in the triclinic space group $P\bar{1}$ (No. 2), and consists of a Co^{2+} cation, $[V_2O_6]^{2-}$ cluster, and bimb ligands (Figure 4). The Co(1) atom

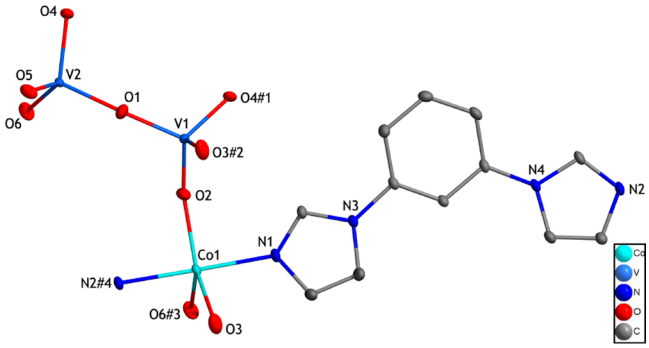

Figure 4. ORTEP diagram (at 30% probability level) of the coordination environment for Co^{II} ions in **2** (for clarity, the H atoms are not shown, symmetry codes: (1) −*x*, −*y*, 1 − *z*; (2) 1 − *x*, 1 − *y*, 1 − *z*; (3) −*x*, 1 − *y*, 1 − *z*; (4) −1 + *x*, *y*, −1 + *z*).

is five-coordination in an elongated hexahedron geometry (Figure 4), defined by three oxygen atoms from three $\{VO_4\}$ tetrahedra and two nitrogen donors from two bimb ligands. The average Co−O bond length is ca. 1.989 Å, and the average Co−N bond length is ca. 2.093 Å, respectively. The O−Co−N angles range from 87.54(10)° to 93.13(10)°. The $[V_2O_6]^{2-}$ is one kind of divanadate anions,[20] and in the $[V_2O_6]^{2-}$ cluster, there are two crystallographically independent V atoms. The V(1) atom, residing in a distorted tetrahedral environment, is coordinated by four bridging oxygen atoms from two $\{CoO_3N_2\}$ hexahedron and two $\{V(2)O_4\}$ tetrahedra. The V(2) atom possesses a distorted tetrahedron achieved by a terminal oxygen atom and three bridging oxygen atoms from one $\{CoO_3N_2\}$ hexahedron and two $\{V(1)O_4\}$ tetrahedra. The

dx.doi.org/10.1021/ic500224m | Inorg. Chem. 2014, 53, 4541−4547

V−O distance range from 1.620(2) to 1.802(2) Å and the average V−O distance is ca. 1.711 Å.

Compound **2** is a novel helical compound based on POMs that possesses a single of double helixes with entanglement nodes in a 3D inorganic−organic network, which belongs to the type III (Scheme 1). Such an intriguing structure can be described in the following three steps: first, the $\{CoO_3N_2\}$ hexahedron, $\{V(1)O_4\}$ tetrahedra, and $\{V(2)O_4\}$ tetrahedra are connected to each other by corner-sharing oxygen atoms to form left- and right-handed helixes with an identical pitch of ca. 10.399 Å. Furthermore, the left- and right-handed helixes are interconnected together through sharing cobalt, vanadium, and oxygen atoms to achieved a double helixes running along the [001] direction (Figure 5). In the second step, each of the

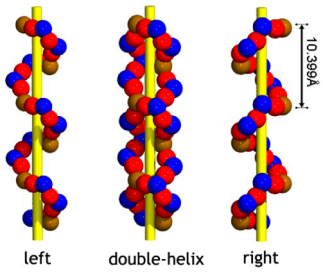

Figure 5. Stereoview of the left-handed, right-handed, and double-helical chains in **2**. Color code: Co, dark yellow; V, blue; O, red. For clarity, only the Co−O−V−O−V−O−Co backbone is shown.

double helixes are further connected by corner-sharing vanadium and oxygen atoms to achieve a $[Co^{II}V^{V}_2O_6]_n$ 2D layer (Figure 6a). Namely, the $\{V(1)O_4\}$ tetrahedra and $\{V(2)O_4\}$ tetrahedra are connected with each other by the corner-sharing oxygen atoms to form $\{V_4O_{12}\}$ clusters, and the $[V_4O_{12}]$ clusters are further linked by Co^{2+} subunits to give rise to the heterometallic layer $[Co^{II}V^{V}_2O_6]_n$. In the third step, as shown in Figure 6b, the adjacent $[Co^{II}V^{V}_2O_6]_n$ layers are connected together by the V-shaped bimb ligands via Co−N bonds to form a 3D inorganic−organic framework. In order to better understand the structure of compound **2**, the topological analysis of the structure has been performed by considering each $[V_4O_{12}]$ cluster as a 5-connected node and each $\{CoO_3N_2\}$ hexahedron as a 6-connected node, and thus, the structure displays (5,6)-network topology with a Schläfli symbol of $(4^3\ 6^7)(4^6\ 6^9)$ (Figure 6c).

Influence of Introducing Ligand on Helical Structures of Cobalt−Vanadate System. Compounds **1** and **2** were synthesized under the identical hydrothermal conditions except for introducing an additional V-shaped bimb ligand into the reaction system of **2**; however, the helix motifs in these two compounds are turned from pair to single entangled double helixes.

We deduce that the structural distinction of **1** and **2** may arise from the difference of the steric hindrance of bimb ligand as well as coordination geometries of metal cations (Figure 7). Namely, in **1**, the Co^{II} ion display six-coordinated octahedral geometry, while in **2**, due to the steric hindrance of bimb ligand, the Co^{II} ion displays five-coordinated hexahedral geometry. Generally, from the view of coronation chemistry, the metal synths with high coordinated number are favored to form the complicated sutures. Therefore, to some extent, this work provides a practical example that the helical structures can be modulated via introducing proper ligands also further verifies that the vanadium oxide polyhedra with multiform coordination geometries (tetrahedrons, square pyramids, trigonal bipyramids, and octahedra) are good synthons for the synthesis of novel helixes.

Analyses of IR and XRPD. As shown in Figure S5 (Supporting Information), the IR spectra exhibit the characteristic peaks of ν(V═O) and ν_{as}(V−O−M) (M = V/Co) at 983, 939, 836, and 648 cm^{-1} in **1** as well as 942, 872, 789, 725, and 642 cm^{-1} in **2**. In addition, the peaks at 3293 and 3437 cm^{-1} can be assigned to the vibrations of water molecules in **1** and the bands in the 1511−1057 cm^{-1} region can be assigned to characteristic peaks of the bimb ligands in **2**.

The XRPD patterns for **1** and **2** are presented in Figure S6 (Supporting Information). The diffraction peaks of both simulated and experimental patterns match well, indicating the phase purities of the two compounds are good.

Cyclic Voltammetry (CV). The polyoxovanadates process the abilities to undergo reversible monoelectron redox processes V^V/V^{IV}, which endows them with attractive electrochemical and electrocatalytic properties.[34−36] To study the electrochemical and electrocatalytic properties of **1** and **2**, the CPEs (**1**− and **2**−CPE) were prepared according to the previous method.[37]

Cyclic Voltammetric Behavior of 1− and 2−CPEs in Aqueous Electrolyte. The cyclic voltammetric behavior for **1**− and **2**−CPE was studied in 1 M H_2SO_4 solution (Figure 8). In the potential range of −0.2 to 1.6 V, both the CPEs exhibit two quasi-reversible redox peaks. The first peaks I−I′ with half-ware potentials $E_{1/2}$ at 1.151 V for **1** and 1.251 V for **2** correspond to one-electron reversible redox processes of vanadium atoms (V^V/V^{IV}).[38] The second peaks II−II′ with half-wave potentials $E_{1/2}$ at 0.646 V for **1** and 0.677 V for **2** correspond to one-electron reversible redox processes of cobalt atoms (Co^{II}/Co^{III}).[39,40]

As shown in Figure 8, when the scan rates varied from 0.04 to 0.08 $V{\cdot}s^{-1}$, the peak potentials change gradually: the cathodic peak potentials shift toward the negative direction and the corresponding anodic peak potentials to the positive direction

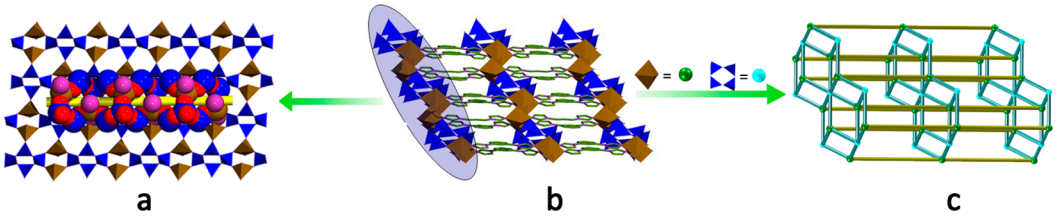

Figure 6. (a) Polyhedral view of the 2D network. (b) Projection of the three-dimensional framework. (c) Topology of 3D network for **2**. Color code: $[V_4O_{12}]$ cluster, blue; $\{Co(H_2O)_2O_4\}$ octahedron, light yellow.

dx.doi.org/10.1021/ic500224m | Inorg. Chem. 2014, 53, 4541−4547

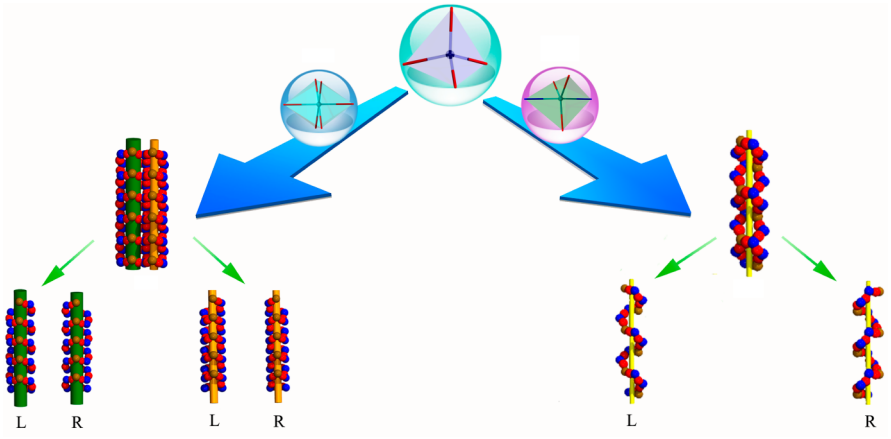

Figure 7. Schematic view of the struture motifs of **1** and **2**.

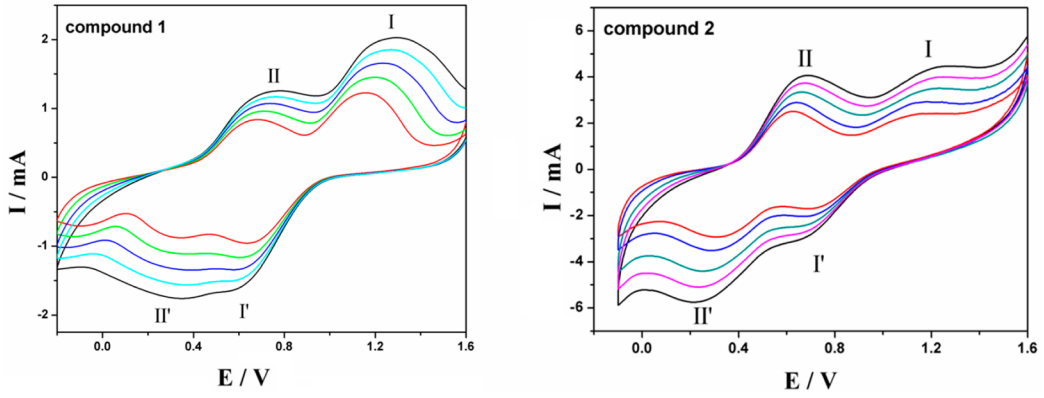

Figure 8. CVs for **1**− and **2**−CPE in 1 M H_2SO_4 solution at different scan rates (from inner to outer: 0.04, 0.05, 0.06, 0.07, and 0.08 $V{\cdot}s^{-1}$).

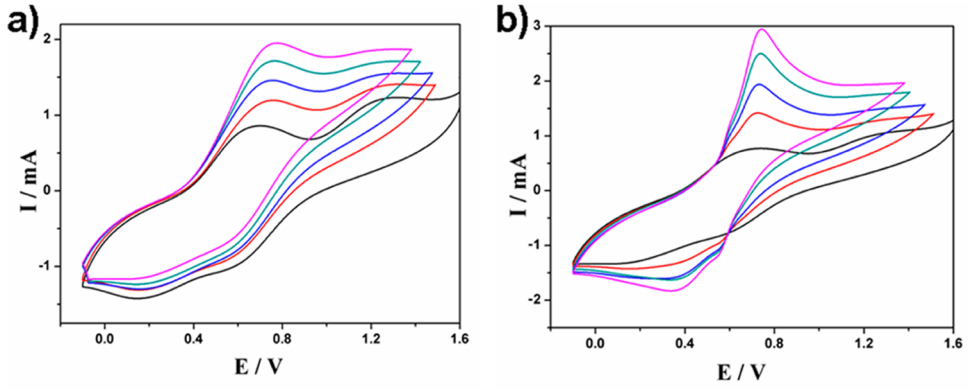

Figure 9. (a) Oxidation of AA (b) oxidation of DA for **2**−CPE, in 1 M H_2SO_4 solution. The concentrations (from inner to outer) are 0.0, 0.4, 0.8, 1.2, 1.6 mM for AA and DA. Scan rate: 70 mV/s. Potentials vs Ag/AgCl.

with increasing scan rates. The peak currents are proportional to the scan rate (Figure S7, Supporting Information), which indicates that the redox processes are surface-controlled and the exchanging rate of electrons is fast.[41]

Electrocatalytic Activity of 1−and 2−CPEs. Ascorbic acid (AA) and dopamine (DA) are vital components in the diet of humans. They are known to take part in several biological reactions and are used clinically in the treatment and prevention of scurvy. Thus, it is significant to be able to detect the AA and DA by an electrochemical method. Herein, the oxidation of AA and DA was chosen as a test reaction to study the electrocatalytic avtivity of **1** and **2**.

As shown in Figure S8 (Supporting Information), after addition of AA and DA, the reduction peaks and oxidation peaks of **1**−CPE are almost unaffected. However, as shown in Figure 9, upon addition of AA and DA, the anodic peak current of both cobalt and vanadium increases obviously, which suggests that the **2**−CPE can catalyze the oxidation of both AA and DA. Although **1** and **2** possess identical inorganic components (Co^{2+} cation and $[V_2O_6]^{2-}$ cluster), the introducing of bimb that is a rich π-electron system into **2** may be favor electron exchanges during the electrocatalytic process, which is a possible main reason why **2**−CPE possesses good electrocatalytic avtivity. Furthermore, the electrocatalytic

dx.doi.org/10.1021/ic500224m | Inorg. Chem. 2014, 53, 4541−4547

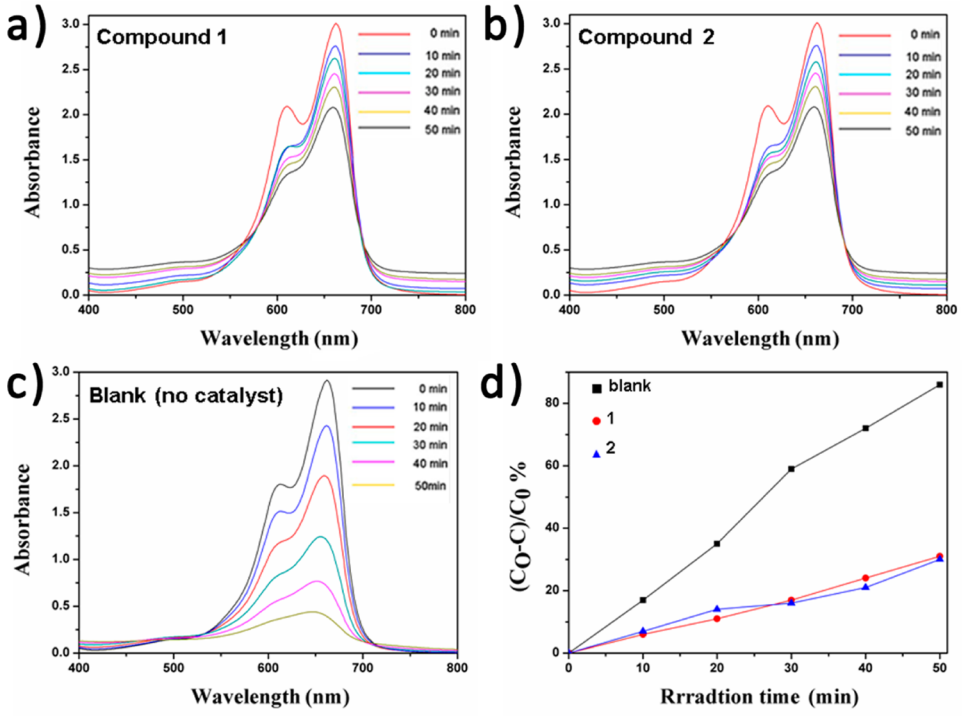

Figure 10. (a) Absorption spectra of the MB aqueous solution during the photodegradation under 250 W Hg lamp irradiation with (a) **1**, (b) **2**, and (c) no catalyst,. (d) Conversion rate of MB (K) vs the irradiation time (t).

efficiency (CAT) of **2**−CPE can be roughly calculated by using CAT formula.[42] The results show that the CAT value toward the oxidation of AA and DA is ca. 100% and 250%, respectively, which suggests that **2** has potential applications in detection of AA and DA.

Photocatalysis Properties. To investigate the photocatalytic activities of these two compounds, the photodecomposition of methylene blue (MB) was evaluated under UV light irradiation through a typical process: prior to photocatalytic experiment, the powder of 150 mg of **1** or **2** was mixed together with 90 mL of a 10.0 mg/L MB solution in a beaker by ultrasonic dispersion for 0.5 h. The mixture was stirred for 2 h to reach the surface−adsorption equilibrium on the particles of **1** or **2**. Then, the mixture was stirred continuously under ultraviolet (UV) irradiation of a 250 W high-pressure Hg lamp at a distance of 4−5 cm between the liquid surface and the lamp. A sample was taken from the mixture every 10 min and then the catalysts of **1** or **2** were removed from this sample by several centrifugations to achieve a clear solution for UV−vis analysis. The results show that the absorbance of the reaction solution decreased as the irradiation time was increased (Figure 10a−c). The decomposition rate of MB (K) can be expressed as $K = (I_0 - I_t)/I_0$, where I_0 represents the UV−vis absorption intensity of MB at the initial time ($t = 0$) and I_t is the intensity at a given time (t). As shown in Figure 10d, the photodegradation ratio of MB over an irradiation time of 50 min decreases from 86% in the absence of **1** or **2** to ca. 31% in the presence of **1** or **2**. The decline in the photodegradation ratio in the presence of **1** or **2** suggests that **1** and **2** restrain the photodegradation of MB. This phenomenon was also observed by Niu[43] and Chen[44] et al. in photodegradation experiments of RhB or MB. The main reasons that **1** and **2** can inhibit the photodegradation of MB may be as follows: (i) compounds **1** and **2** can absorb UV irradiation and therefore decrease the UV irradiation intensity; (2) some weak interactions such as hydrogen bonds between MB and **1** or **2** enhance the chemical stability of MB in solution, which leads to the slow photodegradation of MB substrate.

CONCLUSION

In summary, two compounds have been synthesized under identical hydrothermal conditions except for introduction of additional V-shaped bimb ligands into the reaction system of **2**. Both of the compounds exhibit novel helical structure motifs: compound **1** shows an unprecedented helical disposition type, namely possessing a pair of double helixes with entanglement nodes in a 3D inorganic framework. Compound **2** has a single set of double helixes with entanglement nodes in a 3D inorganic−organic network. The successful isolation of **1** and **2** not only provides intriguing examples of helical compounds based on POMs but also confirms that the vanadium oxide polyhedra with multiform coordination geometries (tetrahedrons, square pyramids, trigonal bipyramids, and octahedra) are good synthons for the synthesis of novel helical compounds, and the helical structures can be effectively modulated via introduction of proper ligands. In hindsight, we can imagine that more new helical compounds could be prepared by replacement of metal segments and/or by appropriate choices of different ligands in the near future.

ASSOCIATED CONTENT

Supporting Information

CIF files, Figures S1−S8, as well as discussions on synthesis and photocatalytic properties. This materials are available free of charge via the Internet at http://pubs.acs.org.

AUTHOR INFORMATION

Corresponding Authors

*: E-mail: mahy017@163.com.

dx.doi.org/10.1021/ic500224m | Inorg. Chem. 2014, 53, 4541−4547

*E-mail: panghj116@163.com.

Notes

The authors declare no competing financial interest.

■ ACKNOWLEDGMENTS

This work was financially supported by the NSF of China (No.21371041 and 21101045), the NSF of Heilongjiang Province (No.B201103), and the Excellent Academic Leader Program of HUST.

■ REFERENCES

(1) (a) Lehn, J. M.; Rigault, A.; Siegel, J.; Harrowfield, J.; Chevrier, B.; Moras, D. *Proc. Natl. Acad. Sci. U.S.A.* **1987**, *84*, 2565. (b) Berl, V.; Huc, I.; Khoury, R. G.; Krische, M. J.; Lehn, J. M. *Nature* **2000**, *407*, 720. (c) Cui, Y.; Lee, S. J.; Lin, W. *J. Am. Chem. Soc.* **2003**, *125*, 6014. (d) Chen, X. M.; Liu, G. F. *Chem.—Eur. J.* **2002**, *8*, 4811. (e) Grosshans, P.; Jouaiti, A.; Bulach, V.; Planeix, J.; Hosseini, M. W.; Nicoud, J. F. *Chem. Commun.* **2003**, 1336. (f) Luan, X. J.; Wang, Y. Y.; Li, D. S.; Liu, P.; Hu, H. M.; Shi, Q. Z.; Peng, S. M. *Angew. Chem., Int. Ed.* **2005**, *44*, 3864.

(2) (a) Nakano, T.; Okamoto, Y. *Chem. Rev.* **2001**, *101*, 4013. (b) Albrecht, M. *Chem. Rev.* **2001**, *101*, 3457. (c) Song, Y.; Yu, J.; Li, Y.; Li, G.; Xu, R. *Angew. Chem., Int. Ed.* **2004**, *43*, 2399.

(3) Sun, C. Y.; Liu, S. X.; Liang, D. D.; Shao, K. Z.; Ren, Y. H.; Su, Z. M. *J. Am. Chem. Soc.* **2009**, *131*, 1883.

(4) Zhang, Z. M.; Li, Y. G.; Yao, S.; Wang, E. B.; Wang, Y. H.; Clérac, R. *Angew. Chem.* **2009**, *121*, 1.

(5) Müller, A.; Peters, F. *Chem. Rev.* **1998**, *98*, 239.

(6) Coronado, E.; Galán-Mascarós, J. R.; Giménez-Saiz, C.; Gómez-García, C. J.; Martínez-Ferrero, E.; Almeida, M.; Lopes, E. B. *Adv. Mater.* **2004**, *16*, 324.

(7) Uchida, S.; Kawamoto, R.; Tagami, H.; Nakagawa, Y.; Mizuno, N. *J. Am. Chem. Soc.* **2008**, *130*, 12370.

(8) Wang, X. H.; Liu, J. F.; Pope, M. T. *Dalton Trans.* **2003**, 957.

(9) Yamase, T. *J. Chem. Soc., Dalton Trans.* **1985**, 2585.

(10) Coronado, E.; Giménez-Saiz, C.; Gómez-García, C. J. *Coord. Chem. Rev.* **2005**, *249*, 1776.

(11) Rhule, J. T.; Hill, C. L.; Judd, D. A. *Chem. Rev.* **1998**, *98*, 327.

(12) Gao, J.; Yan, J.; Beeg, S.; Long, D. L.; Cronin, L. *J. Am. Chem. Soc.* **2013**, *135*, 1796.

(13) Zhao, H. Y.; Zhao, J. W.; Yang, B. F.; He, H.; Yang, G. Y. *Cryst. Growth Des.* **2013**, *13*, 5169.

(14) Zhang, J. W.; Huang, Y. C.; Zhang, J.; She, S.; Hao, J.; Wei, Y. G. *Dalton Trans.* **2014**, *43*, 2722.

(15) Hagrman, D.; Hagrman, P. J.; Zubieta, J. *Angew. Chem., Int. Ed.* **1999**, *38*, 3165.

(16) Soghomonian, V.; Chen, Q.; Haushalter, R. C.; Zubieta, J.; O'Connor, C. J. *Science* **1993**, *259*, 1596.

(17) (a) Liu, C.; Luo, F.; Liu, N.; Cui, Y.; Wang, X.; Wang, E. B.; Chen, J. *Cryst. Growth Des.* **2006**, *6*, 2658. (b) Zhou, J.; Liu, X.; Hu, F. L.; Chen, R.; Zou, H. H.; Fu, W. S.; Liang, G. M.; Chen, Y. *CrystEngComm* **2013**, *15*, 4593. (c) Teng, Y. L.; Dong, B. X.; Peng, J.; Zhang, S. Y.; Chen, L.; Song, L.; Ge, J. *CrystEngComm* **2013**, *15*, 2783. (d) Zhou, J.; Liu, X.; Chen, R.; Hu, F. L.; Zou, H. H.; Wei, M. X. *Dalton Trans.* **2013**, *42*, 5603. (e) Wang, X.; Zhang, M. M.; Hao, X. L.; Wang, Y. H.; Wei, Y.; Liang, F. S.; Xu, L. J.; Li, Y. G. *Cryst. Growth Des.* **2013**, *13*, 3454. (f) Shi, Z.; Feng, S. H.; Gao, S.; Zhang, L. R.; Yang, G. Y.; Hua, J. *Angew. Chem., Int. Ed.* **2000**, *39*, 2325. (g) Qin, C.; Wang, X. L.; Yuan, L.; Wang, E. B. *Cryst. Growth Des.* **2008**, *8*, 2093. (h) Zhang, J.; Hao, J.; Wei, Y. G.; Xiao, F. P.; Yin, P. C.; Wang, L. S. *J. Am. Chem. Soc.* **2010**, *132*, 14.

(18) (a) An, H. Y.; Wang, E. B.; Xiao, D. R.; Li, Y. G.; Su, Z. M.; Xu, L. *Angew. Chem., Int. Ed.* **2005**, *44*, 1. (b) Wang, X. L.; Qin, C.; Wang, E. B.; Su, Z. M. *Chem. Commun.* **2007**, 4245. (c) Sha, J. Q.; Li, M. T.; Sun, J. W.; Zhang, Y. N.; Yan, P. F.; Li, G. M. *Dalton Trans.* **2013**, *42*, 7803.

(19) (a) Lu, C. Z.; Wu, C. D.; Lu, S. F.; Liu, J. C.; Wu, Q. J.; Zhuang, H. H.; Huang, J. S. *Chem. Commun.* **2002**, 152. (b) Wu, C. D.; Lu, C. Z.; Lin, X.; Wu, D. M.; Lu, S. F.; Zhuang, H. H.; Huang, J. S. *Chem. Commun.* **2003**, 1284. (c) Sha, J. Q.; Li, M. T.; Sun, J. W.; Yan, P. F.; Li, G. M.; Zhang, L. *Chem.—Asian J.* **2013**, *8*, 2254.

(20) Lan, Y. Q.; Li, S. L.; Wang, X. L.; Shao, K. Z.; Du, D. Y.; Su, Z. M.; Wang, E. B. *Chem.—Eur. J.* **2008**, *14*, 9999.

(21) Hamilton, E. E.; Fanwick, P. E.; Wilker, J. J. *J. Am. Chem. Soc.* **2002**, *124*, 78.

(22) Fuchs, J.; Mahjour, S.; Pickardt, J. *Angew. Chem., Int. Ed. Engl.* **1976**, *15*, 374.

(23) Day, V. W.; Klemperer, W. G.; Yaghi, O. M. *J. Am. Chem. Soc.* **1989**, *111*, 4518.

(24) (a) Bino, A.; Cohen, S.; Wirguin, C. H. *Inorg. Chem.* **1982**, *21*, 429. (b) Thomas, J.; Agarwal, M.; Ramanan, A.; Chernovab, N.; Whittingham, M. S. *CrystEngComm* **2009**, *11*, 625. (c) Zhang, Y. P.; Haushalter, R. C.; Zubieta, J. *Inorg. Chem. Acta* **1998**, *277*, 263.

(25) Day, V. W.; Klemperer, W. G.; Yaghi, O. M. *J. Am. Chem. Soc.* **1989**, *111*, 5959.

(26) (a) Hou, D.; Hagen, K. S.; Hill, C. L. *J. Am. Chem. Soc.* **1992**, *114*, 5864. (b) Hao, N.; Qin, C.; Xu, Y.; Wang, E. B.; Li, Y. G.; Shen, E. H.; Xu, L. *Inorg. Chem. Commun.* **2005**, *8*, 592.

(27) Hou, D.; Hagen, K. S.; Hill, C. L. *J. Chem. Soc., Chem. Commun.* **1993**, 426.

(28) Chen, Y. H.; Peng, J.; Yu, H. Q.; Han, Z. G.; Gu, X. J.; Shi, Z. Y.; Wang, E. B.; Hu, N. H. *Inorg. Chim. Acta* **2005**, *358*, 403.

(29) Yoshihito, H.; Kumiko, F.; Tamaki, T.; Akira, U. *Chem. Lett.* **2000**, 770.

(30) Koene, B. E.; Taylor, N. J.; Nazar, L. F. *Angew. Chem., Int. Ed.* **1999**, *38*, 2888.

(31) Han, L.; Hong, M. C. *Inorg. Chem. Commun.* **2005**, *8*, 406.

(32) (a) Sheldrick, G. M. *SHELXS-97, Programs for X-ray Crystal Structure Solution*; University of Göttingen: Göttingen, Germany, 1997. (b) Sheldrick, G. M. *SHELXL-97, Programs for X-ray Crystal Structure Refinement*; University of Göttingen: Göttingen, Germany, 1997. (c) Farrugia, L. J. *WINGX, A Windows Program for Crystal Structure Analysis*; University of Glasgow: Glasgow, UK, 1988.

(33) Brown, I. D.; Altermatt, D. *Acta Crystallogr., Sect. B* **1985**, *41*, 244.

(34) Qu, X. S.; Xu, L.; Gao, G. G.; Li, F. Y.; Yang, Y. Y. *Inorg. Chem.* **2007**, *46*, 4775.

(35) Wang, X. L.; Qin, C.; Wang, E. B.; Su, Z. M. *Chem.—Eur. J.* **2006**, *12*, 2680.

(36) Dong, B. X.; Peng, J.; Tian, A. X.; Sha, J. Q.; Li, L.; Liu, H. S. *Electrochim. Acta* **2007**, *52*, 3804.

(37) Zhang, P. P.; Peng, J.; Pang, H. J.; Chen, Y.; Zhu, M.; Wang, D. D.; Liu, M. G.; Wang, Y. H. *Inorg. Chem. Commun.* **2010**, *13*, 1414.

(38) (a) Qi, Y. F.; Wang, E. B.; Li, J.; Li, Y. G. J. *Solid State Chem.* **2009**, *182*, 2640. (b) Qi, Y. F.; Li, Y. G.; Qin, C.; Wang, E. B.; Jin, H.; Xiao, D. R.; Wang, X. L.; Chang, S. *Inorg. Chem.* **2007**, *46*, 3217.

(39) Bassil, B. S.; Kortz, U.; Tigan, A. S.; Juan, J.M. C.; Keita, B.; de Oliveira, P.; Nadjo, L. *Inorg. Chem.* **2005**, *44*, 9360.

(40) Lisnard, L.; Mialane, P.; Dolbecq, A.; Marrot, J.; Juan, J. M. C.; Coronado, E.; Keita, B.; Oliveira, P. D.; Nadjo, L.; Sécheresse, F. *Chem.—Eur. J.* **2007**, *13*, 3525.

(41) (a) Wang, X. L.; Hu, H. L.; Tian, A. X.; Lin, H. Y.; Li, J. *Inorg. Chem.* **2010**, *49*, 10299. (b) Sha, J. Q.; Peng, J.; Liu, H. S.; Chen, J.; Tian, A. X.; Zhang, P. P. *Inorg. Chem.* **2007**, *46*, 11183. (c) Zhang, P. P.; Peng, J.; Pang, H. J.; Sha, J. Q.; Zhu, M.; Wang, D. D.; Liu, M. G.; Su, Z. M. *Cryst. Growth Des.* **2011**, *11*, 2736.

(42) Keita, B.; Belhouari, A.; Nadjo, L.; Contant, R. *J. Electroanal. Chem.* **1995**, *381*, 243.

(43) Niu, J. Y.; Zhang, S. W.; Chen, H. N.; Zhao, J. W.; Ma, P. T.; Wang, J. P. *Cryst. Growth Des.* **2011**, *11*, 3769.

(44) Zhou, S.; Chen, Y. G.; Liu, B.; Li, X. M.; Wang, D. X. *Eur. J. Inorg. Chem.* **2013**, 6097.